Advanced Journal of Chemistry-Section A

Journal homepage: www.ajchem-a.com

Original Research Article

Corrosion Inhibitive Potentials of Some Amino Acid Derivatives of 1,4-Naphthoquinone–DFT Calculations

Timothy Oluwaseun Esan[1,*], Oluwatoba Emmanuel Oyeneyin[2], Abimbola Deola Olanipekun[1], Nureni Ipinloju[2]

[1] *Department of Chemical Sciences, Bamidele Olumilua University of Education Science and Technology, Ikere – Ekiti, Ekti-State, Nigeria*

[2] *Theoretical and Computational Chemistry Unit, Department of Chemical Sciences, Adekunle Ajasin University, Akungba-Akoko, Ondo State, Nigeria*

ARTICLE INFO

Article history

Submitted: 29 July 2022
Revised: 24 August 2022
Accepted: 29 August 2022
Available online: 29 August 2022
Manuscript ID: AJCA-2207-1321
Checked for Plagiarism: Yes

DOI: **10.22034/AJCA.2022.353882.1321**

KEYWORDS

Rusting
Organic corrosion inhibitors
Amino acid derivatives of 1,4-naphthoquinone
Density functional theory
Fukui indices

ABSTRACT

The ability of metallic compounds to be corroded when they react with the environment has been of interest as they are used in various industries and domestic applications. The corrosion inhibitive potentials of some amino acid derivatives of 1,4-naphthoquinone were studied using density functional theory by calculating their electronic properties and reactivity descriptors. The energy band gaps followed the order: E > C > A > F > B > D, suggesting that molecules B and D would react better compared with that of the other molecules. Therefore, their ability to shield metals' surface from rusting is better than others. The charge distribution showed that the compounds have sites that can donate and receive electrons via back donation, a condition that cut out for corrosion inhibition mechanisms very well. Also, the values of the fraction of electrons transferred suggest that the molecules have potential as good inhibitors.

GRAPHICAL ABSTRACT

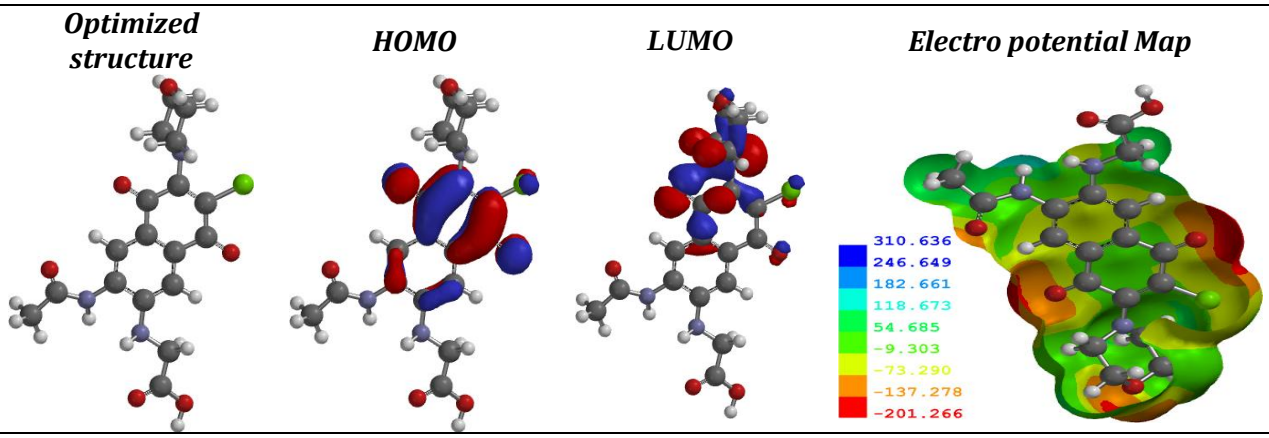

* Corresponding author: Esan, Timothy Oluwaseun
✉ E-mail: timothy.esan@yahoo.com

Introduction

Corrosion of metals occurs when they come in contact with air, hydrogen, and electricity from the environment leading to loss of form, shape, strength, and durability. Also, other adverse effects of corrosion on the environment include loss of lives due to accidents arising from weak metal parts, high cost of production due to high maintenance costs, and property loss [1]. To control the adverse effects of metal corrosion, several compounds have been modeled for their corrosion inhibitive potentials. π-conjugated organic molecules have been investigated and deemed suitable for this purpose as they enable easy movement and flow of electrons [2]. The occurrence of lone pairs of electrons on the hetero atoms (O, S, and N) of some organic compounds encourage organometallic bonding [1,3,4]. Also, the presence of electrophilic moieties in most organic systems enables the acceptance of electrons via back-donation from the metal orbitals [4,5].

The derivatives of 1,4-naphthoquinone amino acid are phenolic compounds in some plant species [6-7]. They have been reported for their bacteriostatic, bactericidal, antiviral, antibiotic, antimalarial, antiplatelet, antihypoxic, antiplasmodial, antiischemic, antianginal, and antitumor activities [8-13]. They have also been reported as fungicides and insecticides [14-15]. This class of compounds has also received interest among material scientists in photo-physical and optical applications [16].

Owing to their extensive π-conjugation and the presence of heteroatoms, their use as corrosion inhibitors could be well explored as the need to continuously search for more anti-corrosive agents remains very important [3, 4]. In almost every area of materials research, the properties of molecules have been predicted using density functional theory (DFT) solely [17-21] and/or in conjunction with experiments [22-24]. This research investigated the corrosion inhibitive ability of amino acid derivatives containing 1,4-naphthoquinone (Figure 1) via DFT calculations. The structures of the derivatives of 1,4-naphthoquinone used in this study have been reported earlier [22].

Computational Method

The modeled molecules were optimized using B3LYP/6-31G* theoretical level with Pulay's D.I.I.S. [25], all on Spartan 14 [26]. The energy gap (E_g) E_{LUMO} and E_{HOMO}, and the global reactivity descriptors were calculated (Equations 1-7) as earlier reported [27].

$$E_g = E_{LUMO} - E_{HOMO} \quad (1)$$

$$I = -E_{HOMO} \quad (2)$$

$$A = -E_{LUMO} \quad (3)$$

$$\eta = \frac{E_g}{2} \quad (4)$$

$$\delta = \frac{1}{\eta} \quad (5)$$

$$\chi = \frac{I+A}{2} \quad (6)$$

$$\Delta N = \frac{xFe - xinh}{2(\eta Fe + \eta inh)} \quad (7)$$

$$f_{k^+} = [\, q_k\,(N+1) - q_k(N)] \quad (8)$$

$$fk^- = [\, q_k\,(N) - q_k(N-1)] \quad (9)$$

$$\Delta f_k(r) = f_k^+ - f_k^- \quad (10)$$

where η_{inh} and χ_{inh} are the parameter descriptors of inhibitors electronegativity and the chemical hardness, respectively, χFe and ηFe represent electronegativity of iron (7.0 eV) and the chemical hardness of the iron (0 eV) [27]. Yao's dual descriptor was used to explain the nucleophilicity and electrophilicity of different atoms of Fukui parameters in Equations 8-10. Q_k (N+1) indicates when the molecule accepts an electron. The ground state or neutral state of the charge in the molecule was represented by q_k (N), while q_k (N-1) represents when the molecule donates an electron [28]. The Fukui functions,

which explain nucleophilic and electrophilic, are represented by fk^{+} and fk^{-} respectively.

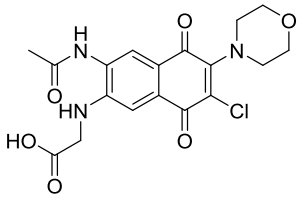

(a) N-[3-(acetylamino)-7-chloro-6-morpholin-4-yl-5,8-dioxo-5,8-dihydronaphtalen-2-yl]-glycine

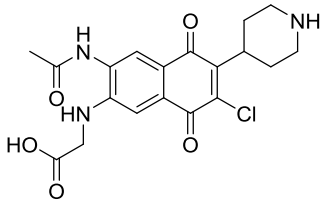

(b) N-[3-(acetylamino)-7-chloro-6-piperidin-4-yl-5,8-dioxo-5,8-dihydronaphtalen-2-yl]-glycine

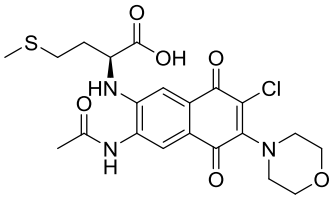

(c) N-[3-(acetylamino)-7-chloro-6-morpholin-4-yl-5,8-dioxo-5,8-dihydronaphtalen-2-yl]-methionine

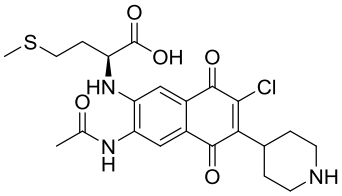

(d) N-[3-(acetylamino)-7-chloro-6-piperidin-4-yl-5,8-dioxo-5,8-dihydronaphtalen-2-yl]-methionine

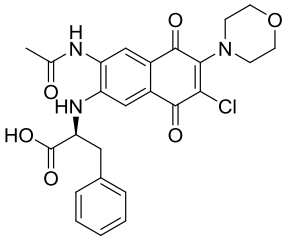

(e) N-[3-(acetylamino)-7-chloro-6-morpholin-4-yl-5,8-dioxo-5,8-dihydronaphtalen-2-yl]-phenylalanine

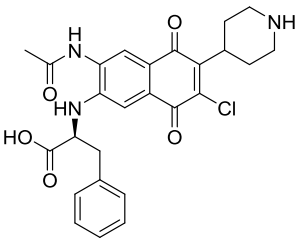

(f) N-[3-(acetylamino)-7-chloro-6-piperidin-4-yl-5,8-dioxo-5,8-dihydronaphtalen-2-yl]-phenylalanine

Figure 1. Structure of the compounds

Results and Discussion

The corrosion inhibition properties of derivatives of amino acid 1,4-naphthoquinone (a-f) were obtained and given in Tables 1, 2, S1-S5. The compounds contain more hetero atoms with π-electrons, which help adsorption and act as nucleophilic centers for π-π reactions. Figures 2, S1-S5 demonstrate the optimized structures of all molecules, HOMO, LUMO, and electrostatic potential maps.

Table 1. The chemical parameters of compounds A–F at the DFT/B3LYP/6-31G(d) theory level

Molecules	E_{HOMO} (eV)	E_{LUMO} (eV)	I (eV)	A (eV)	ΔE (eV)	η (eV)	δ (eV^{-1})	χ(eV)	ΔN
A	-5.68	-2.93	5.68	2.93	2.75	1.38	0.720	4.31	0.978
B	-5.74	-3.12	5.74	3.12	2.62	1.31	0.763	4.43	0.981
C	-5.86	-3.03	5.86	3.03	2.83	1.42	0.704	4.45	0.901
D	-5.87	-3.28	5.87	3.28	2.59	1.29	0.772	4.58	0.934
E	-5.75	-2.85	5.75	2.85	2.90	1.45	0.689	4.30	0.931
F	-5.67	-2.93	5.67	2.93	2.74	1.37	0.729	4.30	0.985

Corrosion inhibition and frontier orbital energies

The molecular orbital energies are used to predict the anti-corrosion potentials of molecular systems. The electron donating ability of a corrosion inhibitor depends on the E_{HOMO} value (Table 1). The molecules A, B, E, and F have a relatively high E_{HOMO}, indicating that the molecules have better electron-donating ability than the others. The halogen substitution (chloride ion) modification to the amino acid derivatives stabilized the E_{HOMO} values, hence lesser electron-donating ability. The molecules A and F gave the highest E_{HOMO} values, which could be the result of an additional pi-electron (π) via the contribution of an electron from phenyl and the amino groups. The compound with greater E_{HOMO} helps slow the anodic process, thereby preventing corrosion [27-31].

Furthermore, a molecule's ability to accept electrons promotes interaction between it and the metal. The low gap between the orbitals (HOMO and LUMO) improves chemical changes or reactivity and the molecule's softness, increasing the potentiality of rusting inhibition [27]. The compounds here have band gaps in the range of significant inhibitors reported by several researchers [4,19] in the following order: E > C > A > F > B > D. The potential characteristics of low energy gaps of the molecules B and D under consideration could result into the relative stabilization of the LUMO and destabilization of HOMO.

To probe into the reactivity of these molecules, the reactivity descriptors like the chemical hardness, softness, and electronegativity were calculated. A molecule is hard if it has high chemical hardness and high energy band gap. Since they are directly related to each other (Equation 4), it follows the same order as in the energy band gap, E > C > A > F > B > D. Low hardness is associated with high softness and vice versa because they are inversely proportional to each other (Equation 5). The order of softness therefore follows, D > B > F > A > C > E. Compound D displayed the highest softness, an indication of its potential to be the best among other compounds in inhibiting corrosion of metals [27, 32]. Electronegativity is the electron-attracting ability . The values ranged from (4.30 – 4.58 eV) for the molecules studied, these values are like those reported in the literature [27, 29, 38]. The number of electrons transferred from the inhibitor to the metal indicates the ability to inhibit the corrosion of metals. The values of ΔN are all less than 3.6 (0.901 – 0.985), a condition for an effective inhibition efficiency displayed by the inhibitors [29].

FMO and electrostatic potential maps

The frontier molecular orbitals and electrostatic potential maps displayed the part of the molecules behaving as donors and acceptors of electrons [34-39], as demonstrated in Figures 2, S1-S5. For molecule A, the HOMO is located on the naphthoquinone ring, including the oxygen and chlorine atoms present. In contrast, the LUMO is located on the morpholine ring and part of the naphthoquinone ring (Figure 2). The highest negative (red color) located within the carbonyl groups in electrostatic potential is an indication that the carbonyl groups are rich in electrons (sites for electrophilic attack). In contrast, the NH_2 and CH_3 groups indicate positive electrostatic potential (blue color), implying a lack of electrons from nucleophilic attack. For B, the HOMO and LOMO are located on the naphthoquinone, including the oxygen and chlorine atoms. Part of the LUMO is extended to the piperidine ring. The negative electrostatic potentials are located in the oxygen areas, while other areas have positive electrostatic potential (Figure S1). The HOMO was spread on the methionine group in compound C, while the LUMO is spread across the naphthoquinone ring and its oxygen atoms. The negative electrostatic

potentials are located in the oxygen, chlorine, and sulfur areas, while other areas have positive electrostatic potential (Figure S2). For D, the HOMO is located on the piperidine ring while the LUMO is spread across the naphthoquinone ring and its oxygen atoms. The electrostatic potentials were observed in A, B, and C (Figure S3). Compound E has its HOMO spread on the naphthoquinone ring and extended to the morpholine ring, while the LUMO is located on the naphthoquinone ring and its oxygen atoms. The electrostatic potentials are similar to that of compound D (Figure S4). For compound F, the HOMO and LUMO were distributed on the piperidine ring and naphthoquinone ring, respectively, and its oxygen atoms possess electrostatic potentials like the other molecules examined (Figure S5). The asymmetrical charge density demonstrated that these compounds possess active adsorption sites for attaching and backward bonding with metals. The adsorption of inhibitor molecules is illustrated in Figure 3.

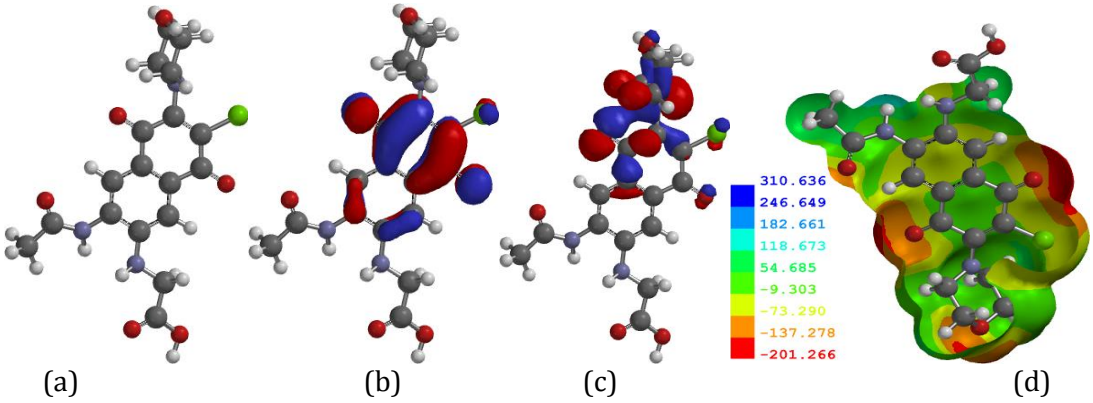

Figure 2. (a) The optimized structure, (b) the highest occupied Molecular Orbital (HOMO), (c) the lowest unoccupied Molecular Orbital (LUMO), (d) Electro potential Map of A

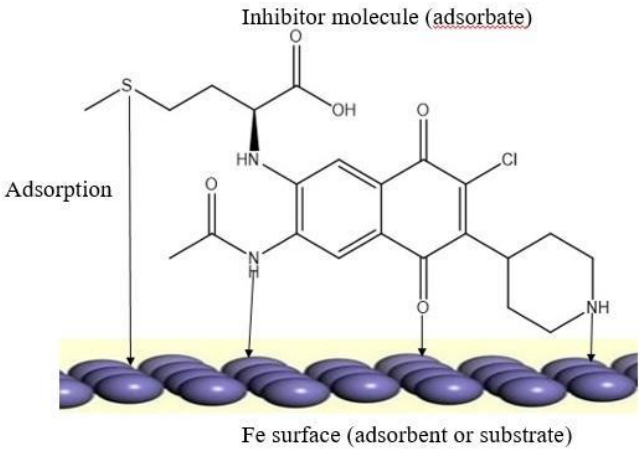

Figure 3. Illustration of the adsorption of the inhibitors on Fe surface

Mulliken charges and fukui functions distributions

Molecules with a Mulliken atomic charge density give information about their reactive sites. Charges computed on the cationic, qk (N-1), neutral, qk (N), and anionic species, qk (N+1) are shown in Tables 2, S1-S5. If the Δfk > 0 (the atom is an electrophile) while nucleophiles have Δfk < 0. Table 2 (compound A) shows that C19 has the highest fk+ (0.042) and a positive fk (0.009), indicating that it favo rs nucleophilic attack. In

contrast, the C23 has the highest fk- (0.035) and a negative fk (-0.017), suggesting that it favo rs electrophilic attack. Compound B has maximum fk+ (0.022) and positive Δfk (0.008) at C20, indicating that it favo rs nucleophilic attack. In contrast, the maximum fk- (0.522) and a negative Δfk (-0.55) was seen at C6, suggesting that it favo rs electrophilic attack (table S1). In compound C (Table S2), the preferred electrophilic attack occurs at C2 with the highest fk+ (0.193) and a positive Δfk (0.353) while nucleophilic attack occurs at C4 with the highest fk- (0.86) and a negative Δfk (-1.704). Compound D (Table S3) has its preferred electrophilic attack occurring at C29 with the highest fk+ (0.547) and a positive Δfk (1.096), while nucleophilic attack occurs at C31 with the highest fk- (1.17) and a negative Δfk (-1.714). C3 in compound E (Table S4) has the highest fk+ (0.498) and a positive Δfk (0.49) which favo rs nucleophilic attack, while the site for an electrophilic attack is at C23 with the highest fk- (0.04) and a negative Δfk (-0.121). In compound F (Table S5), electrophilic attack occurs at C29 with the highest fk+ (1.193) and a positive Δfk (1.198), while nucleophilic attack occurs at C31 with the highest fk- (0.589) and a negative Δfk (-0.89).

Table 2. The selected Calculated Mulliken atomic charges and Fukui functions of compound A

S/N	Atom	$q_K(N+1)$	$q_k(N)$	$q_k(N-1)$	f_k^+	f_k^-	Δfk
1	C1	0.564	0.572	0.589	-0.008	-0.017	0.009
2	N2	-0.706	-0.711	-0.703	0.005	-0.008	0.013
3	C3	-0.177	-0.185	-0.201	0.008	0.016	-0.008
4	O4	-0.472	-0.459	-0.45	-0.013	-0.009	-0.004
5	O5	-0.567	-0.557	-0.541	-0.01	-0.016	0.006
6	C6	-0.28	-0.266	-0.256	-0.014	-0.01	-0.004
7	C7	0.295	0.347	0.402	-0.052	-0.055	0.003
8	C8	0.304	0.321	0.366	-0.017	-0.045	0.028
9	C9	-0.245	-0.218	-0.217	-0.027	-0.001	-0.026
10	C10	0.041	0.041	0.053	0	-0.012	0.012
11	C11	0.332	0.359	0.38	-0.027	-0.021	-0.006
12	C12	0.171	0.306	0.322	-0.135	-0.016	-0.119
13	C13	-0.218	-0.256	-0.231	0.038	-0.025	0.063
14	C14	0.359	0.418	0.426	-0.059	-0.008	-0.051
15	C15	0.044	0.055	0.077	-0.011	-0.022	0.011
16	O16	-0.581	-0.481	-0.44	-0.1	-0.041	-0.059
17	O17	-0.591	-0.476	-0.447	-0.115	-0.029	-0.086
18	N18	-0.474	-0.474	-0.433	0	-0.041	0.041
19	C19	-0.117	-0.159	-0.192	**0.042**	0.033	**0.009**
20	C20	-0.03	-0.035	-0.046	0.005	0.011	-0.006
21	O21	-0.485	-0.467	-0.432	-0.018	-0.035	0.017
22	C22	-0.031	-0.038	-0.0051	0.007	-0.0329	0.0399
23	C23	-0.118	-0.136	-0.171	0.018	**0.035**	**-0.017**
24	N24	-0.727	-0.74	-0.738	0.013	-0.002	0.015
25	C25	0.595	0.599	0.606	-0.004	-0.007	0.003
26	O26	-0.5	-0.477	-0.432	-0.023	-0.045	0.022
27	C28	-0.54	-0.546	-0.559	0.006	0.013	-0.007
28	Cl24	-0.082	0.009	0.128	-0.091	-0.119	0.028

Conclusion

DFT was used to investigate the corrosion inhibitory properties of six derivatives of amino acid 1,4-naphthoquinone from A to F. The compounds' low energy band gap and global hardness, and their high molecular softness,

indicate their ability to inhibit corrosion. Compounds B and D, on the other hand, revealed minimal energy band gaps and high global softness, implying that they are reactive and thermodynamically active inhibitors with the best anti-corrosion capacity. The occurrence of an electron-donating amino group on molecules b and d may indeed explain its minimal energy gap, which necessitates the best corrosion inhibition ability. The compounds can receive electrons from the metal's orbital via back donation and transfer electrons to the metal's vacant orbitals, as shown by the asymmetric charge distribution.

Disclosure statement

The authors reported no potential conflict of interest.

Orcid

Timothy O. Esan 0000-0001-6554-4947
Oluwatoba E. Oyeneyin 0000-0001-5709-0244
Nureni Ipinloju 0000-0002-2683-7146

References

[1] C. Verma, M.A. Quraishi, E.E. Ebenso, *Sustain. Chem. Pharm.*, **2018**, *10*, 134–147. [CrossRef], [Google Scholar], [Publisher]

[2] I.B. Obot, N.O. Obi-egbedi, S.A. Umoren, *Corros. Sci.*, **2009**, *51*, 1868–1875. [CrossRef], [Google Scholar], [Publisher]

[3] Y. Boughoues, M. Benamira, L. Messaadia, N. Bouider, S. Abdelaziz, *RSC Adv.*, **2020**, *10*, 24145–24158. [CrossRef], [Google Scholar], [Publisher]

[4] N.D. Ojo, R.W. Krause, N.O. Obi-Egbedi, *Comput. Theor. Chem.* **2020**, *1192*, 113050. [CrossRef], [Google Scholar], [Publisher]

[5] M. Rbaa, B. Lakhrissi, *Surf. Int*erfaces, **2019**, *15*, 43–59. [CrossRef], [Google Scholar], [Publisher]

[6] P. Ravichandiran, S. Sheet, D. Premnath, A.R. Kim, D.J. Yoo, *Molecules*, **2019**, *24*, 1437. [CrossRef], [Google Scholar], [Publisher]

[7] P. Ravichandiran, M. Masłyk, S. Sheet, M. Janeczko, D. Premnath, R. Kim, B. Park, M. Han, D.J Yoo, *Chemistryopen*, **2019**, *8*, 589–600. [CrossRef], [Google Scholar], [Publisher]

[8] S.P. de Lira, M.H.R. Seleghim, D.E. Williams, F. Marion, P. Hamill, F. Jean, R.J. Andersen, E. Hajdu, R.G.S. Berlinck, *J. Braz. Chem. Soc.*, **2007**, *18*, 440–443. [CrossRef], [Google Scholar], [Publisher]

[9] A.J.M. da Silva, C.D. Netto, W. Pacienza-Lima, E.C. Torres-Santos, B. Rossi-Bergmann, S. Maurel, A. Valentin, P.R.R. Costa, *J. Braz. Chem. Soc.*, **2009**, *20*, 176–182. [CrossRef], [Google Scholar], [Publisher]

[10] K. Bolibrukh, S. Polovkovych, O. Khoumeri, T. Halenova, I. Nikolaeva, O. Savchuk, T. Terme, P. Vanelle, V. Lubenets, V. Novikov, *Sci Pharm.*, **2015**, *83*, 221–231. [CrossRef], [Google Scholar], [Publisher]

[11] M. Monroy-Cárdenas, D. Méndez, A. Trostchansky, M. Martínez-Cifuentes, R. Araya-Maturana, E. Fuentes, *Front. Chem.*, **2020**, *8*, 533. [CrossRef], [Google Scholar], [Publisher]

[12] S. Oramas-Royo, P. López-Rojas, A. Amesty, D. Gutiérrez, N. Flores, P. Martín-Rodríguez, L. Fernández-Pérez, A. Estévez-Braun, *Molecules*, **2019**, *24*, 3917. [CrossRef], [Google Scholar], [Publisher]

[13] M.H. Khraiwesh, C.M. Lee, Y.B. Brandy, E.S. Akinboye, S. Berhe, G. Gittens, M.M. Abbas, F.R. Ampy, M. Ashraf, O. Bakare, *Arch. Pharm.. Res.*, **2012**, *35*, 27-33. [CrossRef], [Google Scholar], [Publisher]

[14] T. Arasoglu, B. Mansuroglu, S. Derman, B. Gumus, B. Kocyigit, T. Acar, I. Kocacaliskan, *J. Agric. Food Chem.*, **2016**, *64*, 7087–7094. [CrossRef], [Google Scholar], [Publisher]

[15] A.K.M.M. Islam, J.R. Widhalm, *Agronomy*, **2020**, *10*, 1500. [CrossRef], [Google Scholar], [Publisher]

[16] K.V. Basavarajappa, Y.A. Nayaka, H.T. Purushothama, R.O. Yathisha, M.M. Vinay, B.J. Rudresha, K.B. Manjunatha, *J. Mol. Struct.*,

2020, *1199*, 126946. [CrossRef], [Google Scholar], [Publisher]

[17] O.E. Oyeneyin, I.A. Adejoro, T.O. Esan, *Phys. Chem. Res.*, **2018**, *6*, 667–683. [CrossRef], [Google Scholar], [Publisher]

[18] S.S. Khemalapure, V.S. Katti, C.S. Hiremath, S.M. Hiremath, M. Basanagouda, S.B. Radder, *J. Mol. Struct.*, **2019**, *1196*, 280–290. [CrossRef], [Google Scholar], [Publisher]

[19] A.U. Rehman, N.A. Morley, N. Amin, M.I. Arshad, M.A. un Nabi, K. Mahmood, A. Ali, A. Aslam, A. Bibi, M.Z. Iqbal, F. Iqbal, *Ceram. Int.*, **2020**, *46*, 29297–29308. [CrossRef], [Google Scholar], [Publisher]

[20] A. Behmanseh, F. Salimi, G.E. Rajaei. *Monatsh. Chem.*, **2020**, *151*, 25–32. [CrossRef], [Google Scholar], [Publisher]

[21] F. Kamali, G.E. Rajaei, S. Mohajeri, A. Shamel, M. Khodadadi-Moghaddam, *Monatsh. Chem.*, **2020**, *151*, 711–720. [CrossRef], [Google Scholar], [Publisher]

[22] I. Buchkevych, M. Kurka, A. Krvavych, N. Monka, V. Novikov, V. Lubenets, *Biointerface Res. Appl. Chem.*, **2021**, *11*, 13903–13910. [CrossRef], [Google Scholar]

[23] E. Golipour-Chobar, F. Salimi, G.E. Rajaei. *Monatsh. Chem.*, **2020**, *151*, 309–318. [CrossRef], [Google Scholar], [Publisher]

[24] K.D. Karjabad, S. Mohajeri, A. Shamel, M. Khodadadi-Moghaddam, G.E. Rajaei, *S.N. Appl. Sci.*, **2020**, *2*, 574. [CrossRef], [Google Scholar], [Publisher]

[25] F. Jensen, *J. Chem. Phys.*, **2001**, *116*, 3502. [CrossRef], [Google Scholar], [Publisher]

[26] Irvine (C.A.), "SPARTAN 14', build 1.01.," 2014.

[27] O.E. Oyeneyin, N.D. Ojo, N. Ipinloju, A.C. James, E.B. Agbaffa, *Chem. Afr.*, **2022**, *5*, 319–332. [CrossRef], [Google Scholar], [Publisher]

[28] R.G. Yang, W. Parr, *Proc. Natl. Acad. Sci.*, **1985**, *82*, 6723–6726. [CrossRef], [Google Scholar], [Publisher]

[29] O.A. Odewole, C.U. Ibeji, H.O. Oluwasola, O.E. Oyeneyin, K.G. Akpomie, C.M. Ugwu, C.G. Ugwu, T.E. Bakare, *J. Mol. Struct.,* **2021**, *1223*, 129214. [CrossRef], [Google Scholar], [Publisher]

[30] F.E. Ani, C.U. Ibeji, N.L. Obasi, M.T. Kelani, K. Ukogu, G.F. Tolufashe, S.A. Ogundare, O.E. Oyeneyin, G.E.M. Maguire, H.G. Kruger, *Sci. Rep.*, **2021**, *11*, 8151. [CrossRef], [Google Scholar], [Publisher]

[31] R. Arulraj, *J. Mol. Struct.*, **2022**, *1248*, 131483. [CrossRef], [Google Scholar], [Publisher]

[32] N.D. Ojo, R.W. Krause, N.O. Obi-Egbedi. *J. Mol. Liq.*, **2020**, *319*, 1–8. [CrossRef], [Google Scholar], [Publisher]

[33] I. Lukovits, E. Kalman, F. Zucchi, *Corrosion*, **2001**, *57*, 3–8. [CrossRef], [Google Scholar], [Publisher]

[34] R. Sukanya, D. Aruldhas, I.H. Joe, S. Balachandran, *J. Mol. Struct.*, **2022**, *1253*, 132273. [CrossRef], [Google Scholar], [Publisher]

[35] C.D. Vincy, J.D.D. Tarika, X.D.D. Dexlin, A. Rathika, T.J. Beaula, *J. Mol. Struct.*, **2022**, *1247*, 131388. [CrossRef], [Google Scholar], [Publisher]

[36] T. Pooventhiran, R. Thomas, U. Bhattacharyya, S. Sowrirajan, A. Irfan, D.J. Rao, *Vietnam J. Chem.*, **2021**, *59*, 887–901. [CrossRef], [Google Scholar], [Publisher]

[37] S.P. Yeddu, P. Thangaiyan, A. Veeraiah, D. Vijay, K.E. Srikanth, A. Irfan, R. Thomas, *Biointerface Res. Appl. Chem.*, **2022**, *12*, 3996–4017. [CrossRef], [Google Scholar]

[38] K. Hussain, N. Amin, M.I. Arshad, *Ceram. Int.*, **2021**, *47*, 3401–3410, [CrossRef], [Google Scholar], [Publisher]

[39] A. Hamil, K.M. Khalifa, A.A. Almutaleb, M.Q. Nouradean, *Adv. J. Chem. A*, **2020**, *3*, 524–535. [CrossRef], [Google Scholar], [Publisher]

HOW TO CITE THIS ARTICLE

Timothy Oluwaseun Esan*, Oluwatoba Emmanuel Oyeneyin, Abimbola Deola Olanipekun, Nureni Ipinloju. Corrosion Inhibitive Potentials of Some Amino Acid Derivatives of 1,4-Naphthoquinone-DFT Calculations. *Adv. J. Chem. A*, **2022**, 5(4), 263-270.

DOI: 10.22034/AJCA.2022.353882.1321

URL: http://www.ajchem-a.com/article_155442.html